Coulomb Forces and Doping in Organic Semiconductors

Brian A. Gregg,* Si-Guang Chen, and Russell A. Cormier†

National Renewable Energy Laboratory, 1617 Cole Boulevard, Golden, Colorado 80401

Received March 5, 2004. Revised Manuscript Received May 26, 2004

A heuristic approach to describing excitonic processes, doping, and transport is developed for all organic semiconductors but with an emphasis on crystalline molecular semiconductors. A simple equation is proposed that semiquantitatively defines "excitonic" semiconductors, XSCs, a classification that includes most organic semiconductors and some inorganic materials. The same electrostatic and spatial factors that cause exciton formation upon light absorption in XSCs, as opposed to the formation of free electron−hole pairs, also control the doping process and carrier transport. Doping studies of XSCs are reviewed with an emphasis on the more recent, quantitative investigations. One conclusion is that most added charge carriers in doped XSCs are not free but rather are electrostatically bound to their conjugate dopant counterions. A superlinear increase in conductivity with doping density is thus expected to be, and apparently is, a universal attribute of XSCs. The interactions between the crystal structure, its dielectric properties, and the doping efficiency are probed via two substitutional dopant molecules in two different crystalline host lattices. An analogy is drawn between purposely doped XSCs and adventitiously doped XSCs such as π-conjugated polymers: in both cases the number of free carriers is a small, and field-dependent, fraction of the total carrier density. The Poole-Frenkel mechanism accounts naturally for the expected interactions between carriers bound in a Coulomb well and an applied electric field. Together with a field-dependent mobility, this mechanism is expected to semiquantitatively describe the conductivity in doped XSCs.

Introduction

One of the great promises of organic electronics is that once the physical requirements for a certain application are clearly understood, synthetic chemists can produce inexpensive compounds having the necessary characteristics. Recent significant advances have been achieved in the fields of organic light-emitting diodes (OLEDs)[1−4] which are now being commercialized, and organic field effect transistors (OFETs) along with their related organic integrated circuits for flexible electronics.[5,6] It was only about 30 years ago that organic semiconductors (SCs) first displaced inorganic SCs in applications such as electrophotography (xerography) and later in laser printers.[7] In the future, organic SCs may eventually replace inorganic SCs in many applications that require inexpensive, large-area semiconductors and that do not require ultrafast switching speeds. Obvious candidate fields for organic SCs are large area lighting with OLEDs[1−4] and organic photovoltaic (OPV) cells.[8−16] The fact that organic SCs are lightweight, flexible, and require only low-temperature processing adds to their potential utility. However, much remains to be learned about the relation between morphological, optical, and electrical properties of these materials.

We present here a brief comparison of organic and inorganic SCs together with a review of doping and transport properties in organic SCs. Finally, we propose a unified approach to understanding the optoelectronic properties of organic SCs. We focus mostly on crystalline molecular semiconductor films because they are the best characterized and easiest to understand. The same basic principles apply also to amorphous molecular semiconductors and to π-conjugated polymers, although these systems suffer from a high degree of energetic (diagonal) and morphological (off-diagonal) disorder. They may also have substantial concentrations of chemical impurities.

Excitonic Semiconductors

There are fundamental differences between conventional semiconductors (CSCs) and excitonic semiconductors (XSCs). Conventional SCs are usually, but not always, inorganic SCs, while XSCs are usually, but not always, organic. The most obvious distinction between CSCs and XSCs is that free charge carriers (electrons and holes) are created directly upon light absorption in CSCs, while electrostatically bound charge carriers (excitons) are formed in XSCs.[10,17] This leads to quite different mechanisms for photoconversion between CSCs and XSCs as described in recent reviews.[8,9] One of the two primary reasons for this difference in mechanism at room temperature is the low dielectric constant, ϵ, of XSCs compared to CSCs. The dielectric constant determines the magnitude of the electrostatic attraction between electrons and holes, and also between these charge carriers and any fixed ionic charges in the lattice such as dopant ions. As described below, the photogeneration of free charge carriers in CSCs, or excitons in XSCs, depends on the square of ϵ.

* To whom correspondence should be addressed. E-mail: brian_gregg@nrel.gov.
† Also at Department of Chemistry, Metropolitan State College of Denver, Denver, Colorado 80204

10.1021/cm049625c CCC: $27.50 © 2004 American Chemical Society
Published on Web 07/13/2004

The other primary difference is the small Bohr radius of carriers, r_B, in XSCs compared to CSCs. For a hydrogen atom in its ground state, the Bohr radius, $r_0 = 0.53$ Å, is the average distance between the electron wave function and the positively charged nucleus. In a semiconductor with hydrogen-like wave functions (such as silicon), the Bohr radius of the lowest electronic state is[18]

$$r_B = r_0 \epsilon \, (m_e/m_{eff}) \tag{1}$$

where m_e is the mass of a free electron in a vacuum and m_{eff} is the effective mass of the electron in the semiconductor (usually less than m_e in CSCs but greater than m_e in XSCs).[17] The effective mass decreases as the carrier becomes more delocalized and its transport becomes more wavelike. Thus, increasing ϵ and decreasing m_{eff} leads to a greater average distance between the charges.

A charge carrier becomes "free" from its Coulomb attraction to an opposite charge if the energy of attraction is less than k_BT, the average thermal energy of the carrier. This occurs when

$$E = (q^2/4\pi\epsilon\epsilon_0)(1/r_c) = k_BT \tag{2}$$

where q is the electronic charge, ϵ_0 (8.85×10^{-14} C/V cm) is the permittivity of free space, and r_c is the critical distance between the two charges. Rearranging eq 2 gives

$$r_C = (q^2/4\pi\epsilon\epsilon_0 k_B T) \tag{3}$$

Excitonic behavior is observed if $r_C > r_B$. In this regime, excitons are formed upon light absorption rather than free electron−hole pairs, and dopants and other charged impurities tend to remain unionized because of the strong Coulomb attraction between the charge carrier and its conjugate dopant or impurity ion. Excitonic behavior is also observed when r_B is greater than the particle radius, but these "quantum-confined" structures will not be considered here.

We define a quantity, γ, that approximately distinguishes between conventional and excitonic semiconductors:

$$\gamma = \frac{r_C}{r_B} \approx \left(\frac{q^2}{4\pi\epsilon_0 k_B r_o m_e}\right)\left(\frac{m_{eff}}{\epsilon^2 T}\right) \tag{4}$$

$\gamma > 1$: excitonic semiconductor

$\gamma < 1$: conventional semiconductor

The inverse temperature dependence shows that if CSCs are cooled to sufficiently low temperature, they will become XSCs. Equation 4 is only a rough approximation for several reasons. First, OSCs conduct mainly through π-orbitals rather than σ-orbitals;[17] thus, they are usually low-dimensional materials: conductivity along one axis is often far greater than along other axes. Therefore, the parameters r_C, r_B, ϵ, and m_{eff} do not have the spherical spatial symmetry implied by the derivation of eq 4. To more accurately describe XSCs, eq 4 would have to be a tensor equation rather than a simple algebraic equation. Furthermore, the effective carrier mass, m_{eff}, is not well-defined in XSCs in which carrier transport typically occurs via a hopping mechanism rather than via delocalized band transport.[17] Finally, ϵ is a bulk quantity and is valid only over distances of many lattice spacings; however, for the tightly bound wave functions that may occur in some XSCs, the effective ϵ can approach its molecular value of 1.0.[18] Despite these approximations, eq 4 is valuable in showing which characteristics are responsible for the distinct differences in behavior between the two types of semiconductors. Although the uncertainty in γ means it cannot distinguish between semiconductors in which γ is near 1, such situations are rare. In general, $\gamma \gg 1$ for XSCs. Note that the factors described in eq 4 and illustrated in Figure 1 do not distinguish between excited state and ground-state processes and, therefore, are valid for both. A schematic representation of the Coulomb attractions in XSCs and CSCs illustrating these concepts is shown in Figure 1.

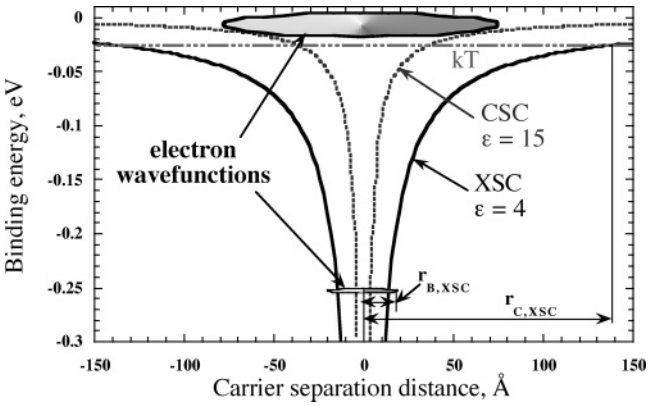

Figure 1. A schematic representation of the fundamental differences between CSCs and XSCs. The calculations assume Coulomb's Law with the positive charge at 0 Å. The relevant distinction is between the size of the wave function (r_B) and the width of the Coulomb potential well at kT (r_C). When the wave function "fits" deep inside the potential well, that is, when $\gamma = r_C/r_B > 1$, excitonic behavior is observed. This general scheme applies to all electrostatic attractions in the semiconductor, not just to photogenerated carriers.

The spatial and electrostatic factors contained in γ account for many of the distinctive features of XSCs relative to CSCs. For example, electrons and holes are created together wherever light is absorbed in CSCs ($\gamma < 1$), while electrons are created on one side of a heterojunction, already separated from the holes created on the opposite side of the heterojunction, by exciton dissociation in XSCs ($\gamma > 1$). This distinctive spatial distribution of photogenerated charges has a powerful influence on the photovoltaic effect: In CSCs the maximum open circuit photovoltage, V_{oc}, is limited to the equilibrium built-in potential, $\emptyset_{bi}$, while in XSCs it is common that $V_{oc} > \emptyset_{bi}$.[8,9] This effect qualitatively distinguishes excitonic PV cells from conventional PV cells, and the same physical phenomena also distinguish doping processes and transport in XSCs from those in CSCs, as described below.

Carrier Density in Organic Semiconductors

The equilibrium free charge carrier density in semiconductors consists of contributions from several sources. The relative importance of the sources can vary substantially depending on the crystallinity and purity of

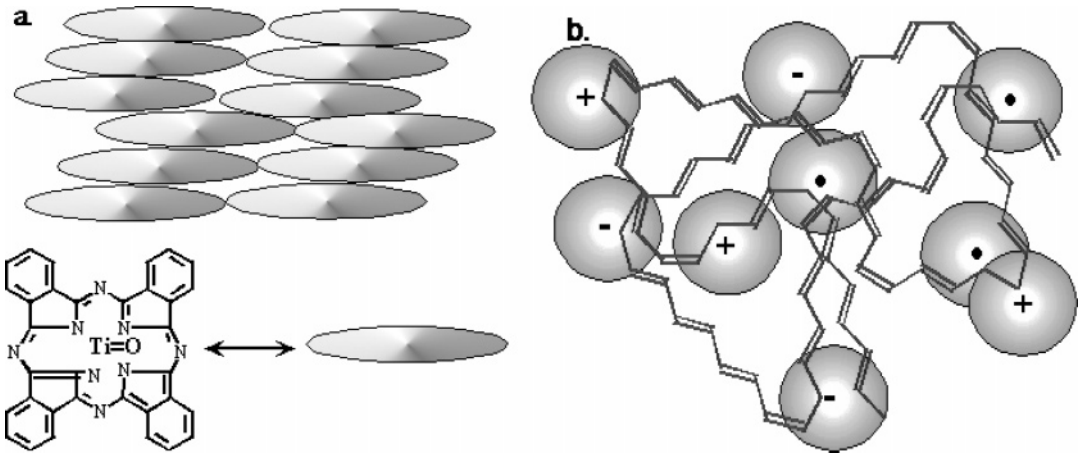

Figure 2. Schematic of (a) the noncovalent disorder of a typical molecular SC that generates relatively few charges and (b) a π-conjugated polymer showing the high charge density generated by the covalent disorder.

the semiconductor and on the type of semiconductor, for example, CSCs, molecular XSCs, or π-conjugated polymeric XSCs. To simplify the discussion, we consider primarily n-doped materials; the relation to p-doped materials should be obvious. First we define several particle densities (chemical concentrations) necessary to describe the free electron density, n_f, at equilibrium: the intrinsic carrier density, n_i, the purposely added dopant density, n_d, and the adventitious dopant density, $n_a = n_{a1} + n_{a2} + ...$ The latter is derived from chemical impurities, crystal imperfections, grain boundaries, bent or twisted π-bonds in a conducting polymer backbone, etc.

The number of *intrinsic* charge carriers in a semiconductor, that is, those created via thermal generation across the band gap is

$$n_i p_i = n_i^2 = N_c N_v \exp(-E_{bg}/k_B T) \qquad (5)$$

where N_c and N_v are the density of electronic states at the bottom of the conduction band and the top of the valence band, respectively, and E_{bg} is the band gap energy. The minimum number of charge carriers that can be present in a SC is n_i since it depends only on equilibrium thermodynamics and is independent of doping density and adventitious impurities. In GaAs, for example, $E_{bg} = 1.42$ eV and $n_i = 2 \times 10^6$ cm^{-3}.[19] Most molecular SCs have substantially larger band gaps than GaAs; however, N_c and N_v are not yet known. Assuming $N_c = N_v \approx 10^{20}$ cm^{-3}, we estimate that common values of n_i for organics are in the range 10^3–10^7 cm^{-3}. In all but the most perfect crystalline molecular XSCs, n_i can be neglected because $n_f \gg n_i$ due to the contributions from n_d and/or n_a. Moreover, as we discuss in the next section, $n_d + n_a \gg n_f$ because $\gamma > 1$; this results in most charge carriers being bound in a Coulomb potential well, while only a small percentage are free.

In terms of n_f, molecular semiconductors such as porphyrins, perylene diimides, and phthalocyanines,[7,17] are very different from π-conjugated polymers such as poly(phenylene vinylene) and poly(thiophene).[16,17] We refer to this as the difference between noncovalent disorder and covalent disorder, respectively (Figure 2). Molecular semiconductors generally have a low equilibrium carrier density ($n_f \approx 10^9$–10^{14} cm^{-3})[11,20] while it is substantially higher in π-conjugated polymers ($n_f \approx 10^{15}$–10^{17} cm^{-3}).[21] The distinguishing feature of π-conjugated polymers is that their conducting backbone is made up of a semi-infinite chain of covalent π-bonds. Entropy, and the morphological constraints of thin film formation, inevitably lead to a large density of electroactive defects caused by twists and bends in the covalent polymer backbone that generate electronic states in the band gap. For example, twisting an individual double bond by 90° results in an unstable diradical that, given the availability of lower energy states in the polymer, will often relax into a more stable anion–cation pair. Bending a bond will destabilize the electrons (or "holes"), also leading to an increased density of charged species and radicals. Even the most pristine polyacetylene film, for example, has numerous charged states and free radicals.[16] Another source of defect carriers arises from the difficulties in purifying high molecular weight polymers. Whereas defects in molecular SCs disrupt only the weak van der Waals bonds between molecules (noncovalent disorder, Figure 2a), defects in π-conjugated polymers break or distort high-energy covalent bonds (covalent disorder, Figure 2b). This explains why n_a in π-conjugated polymers can be many orders of magnitude greater than that in molecular SCs.

Molecular semiconductors, which have no covalent disorder (Figure 2a), still usually have $n_f \gg n_i$ because of morphological defects and chemical impurities. For example, the equilibrium thermal generation of carriers across the band gap (eq 5) may lead to preferential hole trapping at some sites resulting in apparent n-type "doping", or to preferential electron trapping resulting in apparent p-type "doping". This process leads to one strongly bound and one quasi-free (but still electrostatically bound) carrier. Thus, specific organic SCs are usually known in the literature as either n-type (rarely) or p-type (more commonly).[10] However, this distinction is based on adventitious "dopants" (often structural defects) whose number is uncontrolled and whose chemical identity is usually unknown. Because the standard free energy between such bound carriers and their quasi-free counterparts is less than E_{bg}, the density of these carriers can be $> n_i$ at equilibrium (eq 5).

Another issue of importance is the anisotropic nature of organic semiconductors (with the exception of crystal-

line C_{60} and some dendrimers). Molecular SCs are known to conduct predominantly along the $\pi-\pi$ stacking axis, since this is the direction of greatest intermolecular electronic overlap, and less well (often by orders of magnitude) along the two perpendicular axes.[17,22] They may also have substantially different dielectric constants along the different crystal axes. Because of the difficulty of including this important fact in analytical models, it is often neglected. The most highly conducting axis (direction of greatest electronic overlap) of a π-conjugated polymer is usually along the π-conjugated backbone. In theory, crystalline π-conjugated polymers should have high carrier mobilities along the backbone because of their strong electronic coupling.[16] However, actual polymer films are practically isotropic (amorphous) because of their inherent disorder (Figure 2b) and have correspondingly low mobilities.[23−25] In polymer films, the anisotropies can be neglected on a macroscopic level, although they can be significant at the microscopic level.

Doping Organic Semiconductors

The utility of conventional inorganic SCs in the myriad devices of the "information age" depends critically on the ability to precisely dope these materials n-type (electron conducting) or p-type (hole conducting) with high spatial resolution. However, the doping of organic SCs is just beginning to be quantitatively studied.[12,20,26−29] Early studies have shown that doping OSCs (partially oxidizing or reducing them) can increase their conductivity by many orders of magnitude. The observation of metal-like behavior via doping (usually p-type) of molecular semiconductors such as phthalocyanines[22] or π-conjugated polymers such as poly(acetylene), poly(pyrrole), poly(thiophene), and poly(aniline) ultimately gave rise to a new field of study: molecular metals.[16,30,31] There were also early studies of the effect of adding dopant molecules to thin films of OSCs in an attempt to improve their photovoltaic behavior.[32,33]

K. Leo and co-workers recently initiated a series of studies of doping XSCs via cosublimation of an XSC with a dopant molecule such as perfluorinated TCNQ (p-type)[12,26,27] and Pyronin B (n-type).[34] The long-term spatial stability of such doping may be open to question, but this approach has provided a wealth of information. Employing conductivity, Seebeck, and field-effect measurements as a function of temperature, this group has provided a detailed model of doping in several amorphous and polycrystalline XSCs. In their studies, as in others (see below), the conductivity is observed to increase superlinearly with dopant density as the activation energy decreases. They interpret this behavior as supporting their model of shallow (i.e., mostly ionized) dopants. They do not consider the Coulomb force between carriers and dopant ions in their model.

Because of their weak intermolecular forces, doping molecular SCs is quite difficult compared to doping CSCs. In CSCs, the strong covalent, or covalent-ionic, interatomic bonds, along with the relatively high ϵ and large r_B ($\gamma < 1$) contribute to the ease of doping.[28] Bending or breaking the high-energy interatomic bonds at crystal defects and grain boundaries, or incorporating impurities of a valence different than the host, often produce electronic states near enough to the band edges to generate free carriers (similar to what is shown for π-conjugated polymers in Figure 2b). For these reasons, it is difficult to produce truly intrinsic (undoped) CSCs. On the other hand, molecular organic SCs are van der Waals solids; bending or breaking these low-energy intermolecular bonds, or adding different molecules into the lattice, only inefficiently produce free carriers (Figure 2a). Despite concentrations of chemical impurities and structural defects that are often much larger than in CSCs, most molecular SCs are nearly intrinsic.[28] The so-called molecularly "doped" polymers (e.g., triphenylamine "doped" into polycarbonate)[35,36] are similar to *molecular* SCs in this regard, despite the unfortunate use of the term "doping", which in this case has nothing to do with producing free charge carriers.

A little-recognized, although easily demonstrated, fact about p−n junctions is that they are thermodynamically unstable.[37] With n-type dopants on one side and p-type on the other, there is a strong chemical potential gradient that tends to randomize the dopants. The electric field also drives dopants toward intermixing. Except under unusual conditions,[37] therefore, the only factor that allows the continued existence of a p−n junction is the extremely low diffusion coefficient of dopants in the semiconductor lattice. If dopants could diffuse, the junction would disappear. This can be important in CSCs under certain circumstances, however, it is always critically important in XSCs. Because of their generally weak lattice forces, small molecules can diffuse rapidly through a film of XSC. If the dopants are mobile, the electrical properties of the material will change with time, voltage, illumination intensity, etc., and p−n junctions will disappear rapidly as the electrons and holes, as well as their oppositely charged dopant ions, diffuse together and recombine.[20] The most common dopants used in XSCs have been small molecules such as O_2, Br_2, and I_2[7,10,17,22,38] that are incapable of supporting a p−n junction. Larger molecules such as F_4-TCNQ (perfluorinated tetracyanoquinodimethane), TCNQ and TTF (tetrathiafulvalene) have also been employed for doping XSCs.[12,26,27,32,33] The diffusion coefficient of these relatively large molecules is much less than that of the elemental dopants, but it is still too high to produce spatially and temporally stable doping profiles. We describe below what may be the first doping technique that can produce stable junctions in XSCs.

We do not further discuss the doping of XSCs to metallic proportions.[16,22,30,31] In this case, neither dopant diffusion nor drift (in the electric field) is important because the dopant concentration is so high that no substantial concentration gradients can be formed, and no substantial electric fields can be formed in a metal. Here however, we are interested in the semiconducting regime where both diffusion and drift are important.

There have been only a few quantitative studies of the conductivity versus the dopant density in XSCs. However, all of them of which we are aware, both in molecular SCs[12,26,27,39] and in π-conjugated polymers,[16,40−43] exhibit one curious phenomenon: the conductivity increases superlinearly with dopant concentration. We observe this also in our n-doped films of liquid crystalline perylene diimide, PPEEB (Figures 3

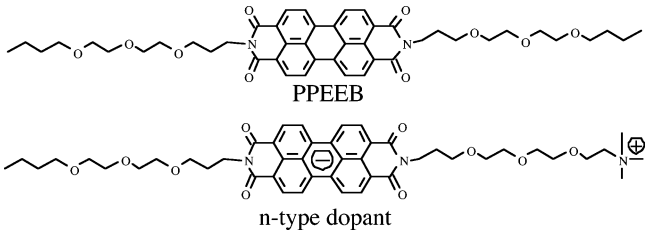

Figure 3. The chemical structure of the host semiconductor, PPEEB, a liquid crystal perylene diimide (that is solid at room temperature), and its associated n-type dopant (the "end dopant"), a reduced derivative of PPEEB with a covalently attached counterion on the end of the side chain. There are no mobile ions in these doped films.

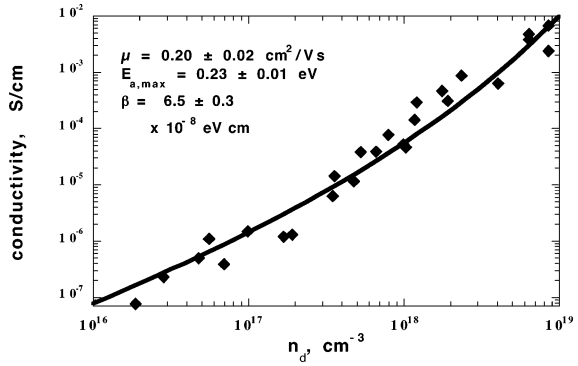

Figure 4. Experimental conductivity of PPEEB films (at a field $F = 0.9$ V/μm) versus dopant concentration; data fit to eq 9. Data are from Gregg et al.[28]

and 4). Something fundamental must underlie this behavior that is independent of crystalline order and XSC type.

Our approach to studying doping in XSCs employs n-doped films of a (liquid) crystalline organic semiconductor, PPEEB (Figure 3).[20,28] PPEEB thin films are well-characterized, highly crystalline (3−10 μm crystallites), and have very low defect densities.[44] To obtain spatially and temporally stable doping in PPEEB films, we synthesized a zwitterionic dopant molecule that is a reduced (for n-type doping) derivative of the host molecule which contains a covalently bound positive countercharge (Figure 3). This molecule is a *substitutional* dopant; that is, it occupies a crystal lattice site identical to the host PPEEB molecule. In contrast, the usual dopants in XSCs are *interstitial*; they reside in normally unoccupied lattice sites and therefore perturb the crystal symmetry. Interstitial dopants are usually far more mobile than substitutional dopants. It is expected, therefore, and it is consistent with all of our observations, that the n-type dopant in PPEEB remains tightly bound in the lattice of its host. The electrical characteristics observed in this model system are expected to also pertain qualitatively to other purposely or adventitiously doped XSCs as described below. In most of these cases, however, the observable phenomena will be further complicated by the presence of mobile ions and by energetic and structural disorder.

Superlinear Increase in Conductivity with Dopant Concentration

We investigated a large number of PPEEB films with dopant concentrations ranging from 34 ppm to 1% ($\sim 10^{16}-10^{19}$ cm^{-3}). The conductivity of these doped films increased *superlinearly* with increasing dopant concentration (Figure 4).[20,28] We present here a simple model that explains the apparent universality of the superlinear increase in conductivity with doping density in XSCs. We assume an isotropic dielectric constant, $\epsilon = 4$ in the undoped films.

Pearson and Bardeen[45] showed that the activation energy for free carrier production, E_a, in doped *conventional* SCs decreases with increasing dopant concentration at low temperature. This occurs because of the many-body electrical interactions between neutral donors, ionized donors, free electrons, and ionized acceptors in crystalline (n-type) doped CSCs. This effect was analyzed further by many groups.[46−48] To discuss this effect (and others) in XSCs, we require four quantities: n_d and n_f (defined previously); the maximum activation energy that occurs for the case of dilute, noninteracting dopants, $E_{a,max}$; and the concentration-dependent activation energy, E_a.

The experimentally observed decrease in E_a with increasing doping density, n_d, leads to a superlinear increase in n_f and therefore conductivity ($\sigma = q\mu_n n_f$ where μ_n is the electron mobility). This is observed only at relatively low temperature in CSCs[46−48] because $E_{a,max}$ is on the order of 10 meV. However, the low dielectric constant and small Bohr radii of XSCs (Figure 1, $\gamma > 1$) generally result in an $E_{a,max}$ of hundreds of meV. Therefore, E_a is expected to control the free carrier density in XSCs, *whether purposely or adventitiously doped*. Decreases in E_a for conductivity in XSCs with increasing n_d have been observed,[12,16,20,26,27,39−43] but unambiguous studies of n_f versus n_d, ideally by Hall effect measurements, are not yet available. In the earlier work on CSCs, values of n_f were known directly from Hall effect measurements. However, we know only n_d and must calculate n_f.

Debye and Conwell[46] discussed three conceptually distinct mechanisms that may lead to a decrease in E_a with increasing doping density:[46] As we showed earlier,[28] it is only the third mechanism that applies to the doped PPEEB films and, we suggest, to other XSC films. The first two mechanisms are governed by n_f, which is usually insignificant compared to n_d in XSCs because $\gamma > 1$. The third mechanism is depicted schematically in Figure 5 where the *polarizability* of the film is shown to increase with the number of electrons in bound but delocalized states near dopant cations, $n_d - n_f \approx n_d$, resulting in an increase in the effective dielectric constant.

Following Debye and Conwell[46] but neglecting n_f,[28] we assume that

$$E_a = E_{a,max} - \beta n_d^{1/3} \tag{6}$$

where β describes the dependence of E_a on the average distance between neutral dopants, $(n_d - n_f)^{1/3} \approx n_d^{1/3}$. Ignoring the miniscule number of intrinsic carriers[20,28] and assuming Boltzmann statistics, the free electron density is

$$n_f = n_d e^{-E_a/kT} \tag{7}$$

and the conductivity is

$$\sigma = q\mu_n n_f = q\mu_n n_d e^{-E_a/kT} \tag{8}$$

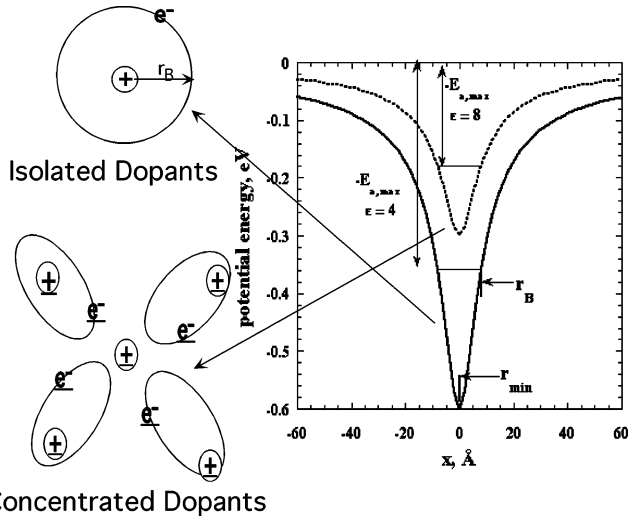

Figure 5. A schematic showing the Coulomb potential around a dopant ion in the LC perylene diimide films. The potential does not go to $-\infty$ at 0 Å because the cation is offset from the electron-conducting pathway (Figure 3). For isolated dopants, the dipole formed by the bound electron orbiting the dopant cation is approximately isotropically oriented. At high concentrations, the ionization of one dopant is energetically stabilized by the ability of surrounding neutral dopants to polarize around the resulting cation. Thus, the polarizability of the *neutral* dopants increases the effective dielectric constant of the film and reduces $E_{a,max}$.

Combining eqs 6 and 8 leads to

$$\sigma = q\mu_n n_d \exp\{(-E_{a,max} + \beta n_d^{1/3})/kT\} \quad (9)$$

This model is expected to be valid for low to moderate doping levels where $n_d^{-1/3} \gg r_B$. A good three-parameter fit to the data was obtained with eq 9 and is shown in Figure 4. The obtained free carrier mobility value of 0.2 cm^2/Vs is reasonable for a highly ordered XSC at $F = 0.9$ V/μm and is similar to the values obtained from our ongoing Hall effect and transport measurements. However, we are assuming that μ_n is a constant in this analysis while, in fact, it may be a function of n_d. Finally, the value of $E_{a,max} = 0.23$ eV at $F = 0.9$ V/μm is close to that expected from an extrapolation of our calculation at zero field strength, $E_{a,max} = 0.36$ eV.[28] To a first approximation, $E_{a,max}$ at zero field strength may be of similar magnitude to the singlet exciton binding energy because they both arise from the same forces, although their geometrical constraints are somewhat different.

Our model assumes Boltzmann statistics. This is valid in semiconductors if the average electrochemical potential of charge carriers, the Fermi level (E_f), is more than k_BT below the conduction band edge, which is certainly true in our case. Therefore, we can relate eq 7 to its more common semiconductor analogue which employs Fermi-Dirac statistics:

$$n_f = n_d e^{-E_a/kT} = N_c e^{(E_c - E_f)/kT} \quad (10)$$

This shows that the free carrier density increases exponentially as E_f approaches the conduction band energy, E_c. If we set $E_c = 0$ as an energy reference point, this can be rearranged to

$$E_a - E_f = k_BT \ln(n_d/N_c) \quad (11)$$

Equation 11 shows that the Fermi level in the doped PPEEB films is below E_a (that is, it is further from E_c) because the density of added dopants is only a small fraction of the density of conduction band states.

No Shallow Dopants in XSCs

The superlinear increase in conductivity observed with increasing doping concentration in the LC perylene diimide films is expected to be, and apparently is, a universal attribute of excitonic semiconductors. This follows directly from the characteristics that define XSCs:[8,9] the strong, long-range, electrostatic attraction between opposite charges, and the relatively localized wave functions of the charge carriers (leading to $\gamma > 1$). The binding energy between opposite charges in PPEEB films decreases with increasing dopant concentration because of the increasing polarizability of the film (Figure 5). One further conclusion from these results is that *it is probably impossible to produce shallow (i.e., mostly ionized) dopants in XSCs*, independent of the chemistry or potentials of the dopant and host. This follows because the binding energy of the charge carrier is determined by the spatial and electrostatic effects contained in γ, not by the difference in potential between the dopant and its respective band edge. In the doped perylene diimides, the dopant redox potential was at the conduction band edge (Figure 3), that is, identical to that of the host. Nevertheless, the charge carrier was localized near the dopant molecule because of the Coulomb force. If the dopant redox potential lies *outside* the band gap of the host, the charge carrier will still relax to the band edge and then be localized near neighboring molecules because of the Coulomb force. If the dopant redox potential lies *inside* the band gap of the host, the charge carrier will be even more localized than in the previous two cases. Dopants can become shallow in typical XSCs only at high dopant density where the film's effective dielectric constant increases and the film's behavior approaches that of a CSC or of a molecular metal rather than a semiconductor. When CSCs are cooled far enough to become XSCs, many of their charge carriers also become localized in the Coulomb wells near the dopant atoms.[45,46]

Variations on Dopant and Host Design

Variations of the original dopant molecule (the "end dopant", Figure 3) and the host were designed to clarify the morphological and electrical effects that control the doping efficiency: defined as the percentage of free carriers formed per added dopant molecule. The powerful influence of the Coulomb attraction between the dopant electron and the covalently bound positive charge on the dopant molecule was an important design criterion of the original dopant. Putting the covalently bound positive charge as far away as possible from the electron in the aromatic ring (Figure 3) was an attempt to minimize the Coulomb force and thereby maximize the doping efficiency. This compound was designed and synthesized before we knew the crystal structure of PPEEB. To test the effect of changing the Coulomb force, we also synthesized the "middle dopant" (Figure

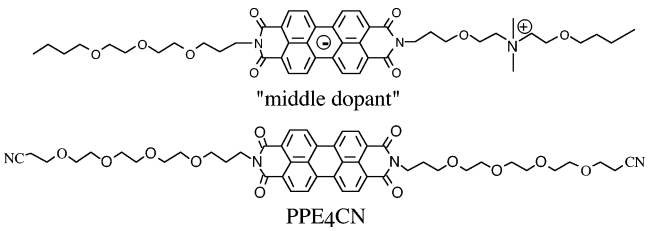

Figure 6. The chemical structures of the "middle dopant", with the positive charge in the middle of the side chain, and PPE_4CN with cyano groups on the ends of the side chains.

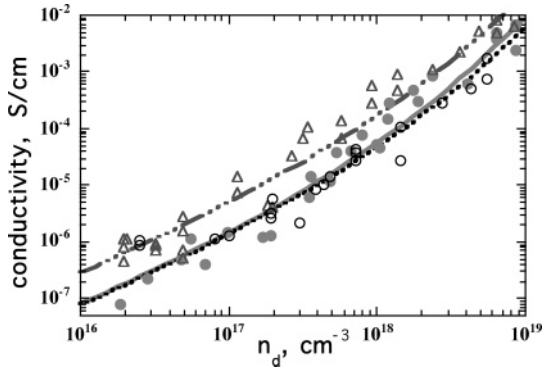

Figure 7. Conductivity versus dopant concentration in three different cases: the end dopant in PPEEB (solid circles, solid fit line, same data as shown in Figure 4), the middle dopant in PPEEB (open circles, dashed fit line), and the end dopant in PPE_4CN (open triangles, dot−dashed fit line). The "intrinsic" conductivity of PPE_4CN has been subtracted from its doped conductivity (see below). The fits are to eq 9; the fit parameters are given in Table 1.

6) with the positive charge in the middle of the side chain. Then, in an attempt to increase the dielectric constant of the film, we synthesized PPE_4CN (Figure 6), an LC perylene diimide quite similar to PPEEB but containing a highly polar cyano group at the end of each of its side chains.

The synthesis and purification of PPE_4CN was described previously,[44] while that of the middle dopant is described here in the Experimental Section. Extensive studies of the end dopant in PPE_4CN and of the middle dopant in PPEEB were carried out and compared to the end dopant in PPEEB. Conductivity versus dopant concentration results for the three combinations are shown in Figure 7. Although there are differences between the data sets, they are smaller than expected for what we at first thought would be substantial changes in the Coulomb force.

To understand these relatively slight changes in doping efficiency with structure, it is necessary to know the crystal structure of the films (Figure 8).[44] Films of PPEEB and PPE_4CN both form a highly oriented, layered structure similar to a liquid crystal smectic C phase (although both are solids at room temperature). The long axis of the molecules are quasi "end-on" to the substrate but tilted in both dimensions (x and y) perpendicular to the substrate normal (z).[44] The $\pi-\pi$ stacking axis, that is, the axis of highest conductivity, is parallel to the substrate plane (Figure 9). The structures of PPEEB and PPE_4CN films are almost identical except for the slight difference in side chain length. Apparently, the highly polar cyano groups on the ends of the side chains in PPE_4CN do not noticeably

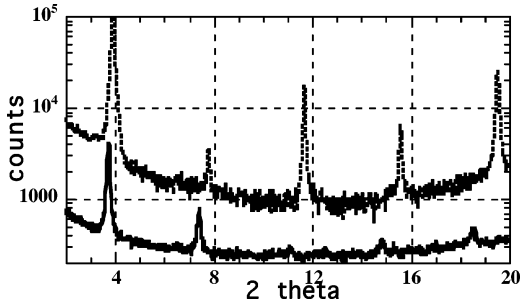

Figure 8. XRD spectra of thin films on glass of PPEEB (dashed line, offset for clarity) and PPE_4CN (solid line).

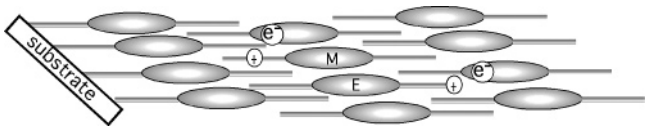

Figure 9. A schematic of the doped PPEEB (and PPE_4CN) films consistent with the measured crystal structure. The large tilt angle of the aromatic rings relative to the substrate minimizes the electrostatic difference between the middle dopant (M, Figure 6) and the end dopant (E, Figure 3) and their respective dopant electrons.

perturb the crystal structure compared to the much less polar PPEEB. PPE_4CN is slightly more dense than PPEEB, 1.34 g/cm^3 compared to 1.27 g/cm^3, presumably because of the electrostatic attraction between the dipolar cyano groups.

The crystal structures show that the side chains of both LC perylene diimides are interdigitated. Furthermore, the core π-rings are tightly stacked upon one another (with a 3.4 Å spacing) in a stacking direction parallel to the substrates. This structure occurs on all substrates we have tested, from glass to highly oriented pyrolytic graphite.[44] Only in *monolayer* films do the π-rings lay flat on the substrates.[49] Possible reasons for this behavior have been discussed.[44] In thin films, the planar aromatic core of the perylene diimides has a total tilt angle of ca. 47° relative to the $\pi-\pi$ stacking axis. This is shown in a two-dimensional representation in Figure 9 that explains the lack of significant difference between the end dopant and the middle dopant.

Our original considerations for dopant design centered on the molecule itself, especially on its ability to fit securely into the host lattice as a substitutional dopant. However, once in the solid state, the dopant electron is free to move to the position of lowest free energy in the lattice. This will be near a positive charge because of the dominance of the Coulomb force at equilibrium. Once the crystal structure is known, the electron's minimum energy location(s) can be estimated (Figure 9), and they are not on the dopant molecules. Therefore, placing the positive charge as far as possible from the electron on the π-system in the dopant *molecule* (Figure 3) was not an effective strategy; in the solid, the electron will move to a molecule on a different stack in order to minimize the energy between it and the positive charge on the dopant molecule. The middle dopant has properties almost identical to the end dopant because, in this case, the electron can closely approach the positive charge by moving to a different molecule in the same or an adjacent stack.

Because the positive charge in all cases is located in the side chain phase, rather than in the conducting $\pi-\pi$

Table 1. Fitting Parameters Obtained from Fitting the Data in Figure 7 to Eq 9

dopant in host	mobility, $cm^2/V\ s$	$E_{a,max}$, eV	$\beta \times 10^{-8}$ eV cm
end-D in PPEEB	0.20 ± 0.02	0.23 ± 0.01	6.5 ± 0.3
mid-D in PPEEB	0.20 ± 0.03	0.23 ± 0.02	6.0 ± 0.5
end-D in PPE_4CN	0.05 ± 0.02	0.16 ± 0.02	6.0 ± 0.8

stacks, the Coulomb potential well in which the electron resides is rounded at the bottom rather than going to $-\infty$ (Figure 5). The electron is also delocalized over a number of host molecules at room temperature because of the high crystallinity and strong intermolecular electronic interactions of the LC perylene diimides.[28] The extent of equilibrium electron delocalization is expected to be at least ~5 molecules ($r_b \geq$ ~9 Å) centered around the minimum energy point (Figure 5), according to recent EPR studies.[50] In sum, because of the large tilt angle of the molecules relative to the substrate in the layered films, and because of the electron delocalization, there are no significant differences between doping PPEEB with the end dopant and the middle dopant (Figures 7 and 9).

Dipoles, Dielectric Constants, and PPE_4CN

We initially thought, in analogy to electrochemical systems, that by adding cyano groups to the side chains (to make PPE_4CN, Figure 6), we could increase the dielectric constant of the SC film, somewhat like replacing hexane ($\epsilon = 2$) with butanenitrile ($\epsilon = 20$). But the analogy to solution is false. Because molecules in the solid cannot physically reorient, a high-dielectric liquid can become a low-dielectric solid when frozen, albeit one with a large fixed dipole density. Upon solidification, the dielectric constant changes from being a function mainly of the fluid dipoles in solution to being a function of the polarizable electrons in a solid. When considering an ~1 ns electron hopping process for the conductivity, as may be expected in the LC perylene diimide films, the relevant dielectric constant is that at ~1 GHz. At this frequency in a solid, primarily loosely bound or unbound electrons contribute to the dielectric properties. Higher applied fields lead to faster hopping and therefore higher relevant frequencies for the dielectric constant. For these reasons (in hindsight), the difference between PPEEB and PPE_4CN is expected to be small at high electric fields, and may be only slightly greater at low fields (Figure 7). In sum, the small increase in dielectric "constant" between PPEEB and PPE_4CN, and corresponding decrease in $E_{a,max}$ (Table 1), is related to the polarizable π-electrons on the cyano groups rather than to their large static dipoles. The static dipoles do play a role in transport, but it is mostly deleterious: they decrease the electron mobility (Table 1, and discussed further below). However, they are also responsible for some unusual behavior in *undoped* PPE_4CN that we discuss first.

The conductivity of undoped PPEEB is at the lower limits of our measurement capabilities, approximately 10^{-12} S/cm. When doped n-type, it reaches $\sigma = 10^{-2}$ S/cm at 1 mol % dopant.[20] However, the conductivity is air-sensitive; when exposed to air σ decreases several orders of magnitude and then remains constant for at least six months. The conductivity regains most of its original value if the film is later placed in a vacuum or under an inert atmosphere. This is consistent with the reversible compensation (removal of charge carriers) of the n-type film by an acceptor (p-type dopant), namely O_2. (We showed that other components of air, H_2O and CO_2, had no effect on σ.) Alone among our LC perylene diimides however, PPE_4CN has a substantial and *air-stable* conductivity in the undoped state, as long as it is in the red phase.

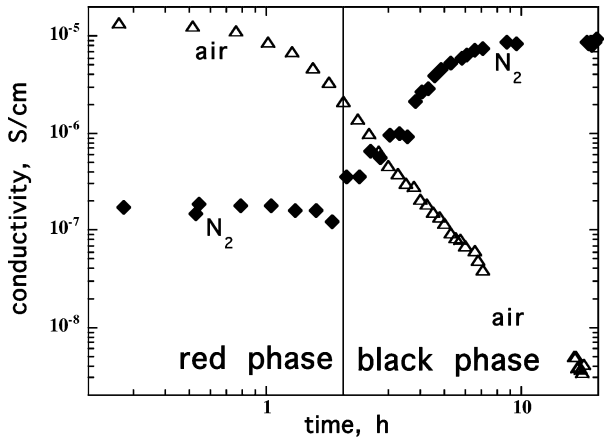

Figure 10. The change in conductivity of *undoped* PPE_4CN as it undergoes the red-to-black phase transition in air and in an N_2 glovebox.

Both PPEEB and PPE_4CN, as well as other LC perylene diimides, form a polycrystalline but relatively disordered phase when first spincoated.[44,51,52] This phase, which is red, spontaneously self-organizes into a black phase over several hours. The black phase is more highly ordered as seen in XRD measurements[44] and much more highly fluorescent[51] than the red phase. In n-doped films of PPEEB, the conductivity increases 3−10-fold during the red-black phase transition, presumably as traps disappear and the electron mobility increases.[20] In striking contrast to the behavior of PPEEB, PPE_4CN in the undoped red phase is quite highly conductive even in air ($\sigma \approx 10^{-5}$ S/cm, ~7 orders of magnitude higher than PPEEB). Furthermore, σ is stable in air as long as the red phase is maintained (up to two weeks in some samples). If the film is removed from air, σ *decreases* by ~100 fold indicating a natural *p-type* doping in PPE_4CN although its π-system is identical to PPEEB. Moreover, σ *decreases* by ~4 orders of magnitude in air upon the red-to-black phase transition (Figure 10). Almost the opposite behavior is observed under an inert atmosphere: $\sigma \approx 10^{-7}$ S/ cm in the red phase and it *increases* by ~100 fold during the red-black phase transition (Figure 10) and remains ~7 orders of magnitude higher than PPEEB. This curious behavior may be qualitatively explained by the unusually high dipole density in this material.

The cyano groups in PPE_4CN have a partial negative charge at the ends of the side chains and a partial positive charge just "inside" of it. In a relatively disordered environment (the red phase), these dipoles may orient toward certain molecules and thus promote the formation of charge carriers on them via electrostatic stabilization (equivalent to locally decreasing the effective E_{bg} in eq 5, see Figure 11). To preserve electroneutrality, an equal number of countercharges must be created. One of the two carrier types is usually more deeply trapped than the other, and therefore less mobile.

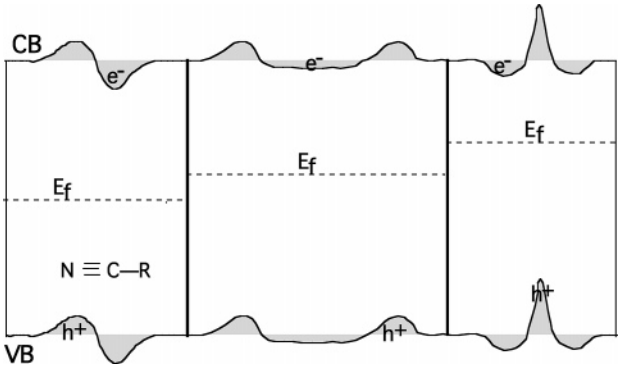

Figure 11. Schematic of the potential fluctuations in conduction and valence band energies (CB and VB respectively) and changes in Fermi level caused by the presence of dipoles. Electrons and holes are represented by e^- and h^+, respectively. The cyano group is employed for illustration (left); it has a partial negative charge on nitrogen and a partial positive charge on carbon. The effect of an isolated dipole is depicted at left. In the more common case in which one carrier is more deeply trapped than the other (middle and right panels), the free carrier density is higher than the intrinsic density ($n_f > n_i$). Even stronger dipoles are caused by bound full charges in the XSC (Figure 2b).

The observed conductivity is proportional to the product of the number of *free* carriers and their mobility ($n_f\mu_n$ for electrons, $p_f\mu_p$ for holes). We suggest the following explanation for the results shown in Figure 10: In the red phase of PPE_4CN, the dipole-generated holes must be on average less deeply trapped than electrons; therefore, the conductivity is dominated by holes. In a N_2 atmosphere, however, many of the potentially free holes are strongly attracted to the bound electrons rendering them less mobile. Exposure to air causes some of the electrons to react with O_2, forming O_2^- and resulting in an increased density of weakly bound holes and a higher conductivity in air than in N_2 (left side of Figure 10). Later, when PPE_4CN crystallizes into the black phase, the number of morphological defects decreases and the dipole field reorganizes. The results in Figure 10 show that the crystallization process results in conductivity dominated by dipole-generated electrons rather than holes. In this phase, therefore, σ decreases substantially in air because O_2 removes some of the mobile electrons (right side of Figure 10). The conductivity increases under N_2 during the phase transition either because of the increased number of dipole-generated electrons (Figure 11), their increased mobility, or both.

This is a reasonable explanation for the unusual behavior of the highly polar PPE_4CN films, but it is still speculative. There are very few examples known of other highly dipolar organic SCs so the data are too sparse to make definite conclusions. Nevertheless, higher dipole densities in an organic solid should result in higher equilibrium charge carrier density *if* one carrier is more deeply trapped than the other as shown in Figure 11.

Figure 11 shows in simplified fashion the changes in E_f that may be induced by dipoles, or native charges, in XSCs. On the left side the effect of a single dipole is shown. Since it stabilizes holes and electrons by the same amount, there is no change in E_f from the intrinsic case and therefore no change in n_f. But the band edge fluctuations shown in the middle and the right side result in dipole-induced holes more deeply bound than the electrons. This causes E_f to move toward the conduction band, resulting in n-type conductivity ("doping"). Actual XSCs that contain dipoles, individual charges, and several different types of trap states are more complex.

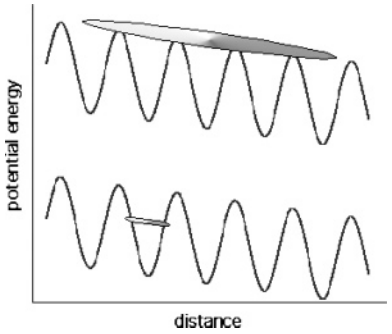

Figure 12. Schematic showing the effect of potential fluctuations on the carrier mobility under an applied field. Ovals represent the electron wave functions. When the spatial extent of the electron wave function ($\approx 2r_B$) is smaller than the scale of the potential fluctuations (lower graph), the carrier mobility is greatly inhibited and becomes field-dependent.

Potential Fluctuations and Carrier Transport

Fixed dipoles, or any other kind of spatial fluctuations of the potential, can interfere with the transport of carriers in XSCs.[23−25,35,36,53] Again, this is a function of the electrostatic considerations contained in γ. If the electron wave function is delocalized ($2r_B$) over a distance far greater than the scale of the potential fluctuations in space (GaAs is a good example), the electron "sees" only the average potential and is thus unaffected by the local fluctuations (Figure 12, upper plot). But if the electron is localized on a scale smaller than the potential fluctuations, the electron must surmount, or go around, each potential barrier it encounters (Figure 12, lower plot). This greatly decreases the mobility compared to the more delocalized case, and also makes it dependent on the applied field (see below). Given the usually low values of $2r_B$ in XSCs (maybe 5−50 Å), almost any adventitious or purposely added dipoles or charged species will tend to reduce the carrier mobility and make it field-dependent.

Field Dependence of the Carrier Density

As described above, the spatial and electrostatic effects expressed in γ have a major influence on the charge generation mechanism in XSCs, both via light absorption and via doping. The Coulomb forces ensure that most carriers are bound to a nearby countercharge. It is anticipated then that γ should also play an important role in measurements of the conductivity versus applied field for two reasons: by controlling the number of *free* charge carriers, n_f, and by causing the carrier mobility to become field-dependent as detailed in the next section and mentioned briefly above (Figure 12). The electrical current in an XSC can be limited by many factors:[17] carrier transport through the bulk,[24,54−56] potential barriers at crystallite grain boundaries,[57] injection from the electrodes,[58] space charge limitations,[21,59−62] etc. Models of carrier transport in XSCs can be highly complex and there is no agreement yet on the

relevant assumptions to be included in such models. Considering what was described above, however, we suggest that one important concept has been overlooked in existing models: *the number of free bulk carriers, n_f, is expected to be an increasing function of applied field, F, in many XSCs*, whether purposely or adventitiously doped, because $\gamma > 1$. We are not referring to injected carriers, n_{inj}, whose number is obviously field-dependent, but to n_f. In some cases, this can have a major impact on the interpretation of experimental results.

When measuring the conductivity, n_f and μ_n almost always occur together in the relevant equation (e.g., eq 8), and they are often simply referred to as the "$n\mu$ product". It can be difficult to distinguish experimentally between changes in n_f and changes in μ_n. A concept called "effective mobility" is sometimes introduced that, in essence, assumes n_f is fixed and that therefore any changes in conductivity with temperature, applied voltage, etc. can be ascribed to the effective mobility. This unfortunate assumption can result in serious errors in interpreting experimental results, especially in XSCs. When characterizing a newly synthesized organic material, for example, a decrease in the equilibrium n_f compared to a known material may be misinterpreted as a decrease in μ_n. While the first would be beneficial for photovoltaic applications, the second would be detrimental. Misinterpreting a beneficial change as detrimental is far worse than admitting that one can only measure the $n\mu$ product. Ideally, one should unambiguously distinguish between n_f and μ_n, but this is not always possible with existing techniques. Arguably the best technique would be measurements of the Hall effect.[17] However, Hall effect measurements have not been reliable in XSCs so far because of sample geometry problems, low carrier density, and anisotropic conductivity effects. Mobility measurements in a field effect transistor (FET) geometry[5,6,54] and measurements of the time-of-flight (TOF) transition time[36,63] are some of the best available methods to estimate μ_n in XSCs. However, they are accurate primarily in materials where n_f is very small. The interpretation becomes more ambiguous as n_f increases.

The influence of the Coulomb force is pervasive in XSC films. Therefore, the results obtained from the doped LC perylene diimides discussed above should be applicable to other doped XSC films insofar as only electrostatic forces are considered. Generalizing, therefore, from the results of the doped LC perylene diimide films, we propose several principles for doped XSC films: (1) *Each equilibrium charge carrier* produced in the bulk, whether free or bound, whether originating from n_i, n_d, or n_a, *must be counterbalanced by an opposite charge* to maintain overall electrical neutrality. This opposite charge may be fixed in the lattice (such as a dopant ion), have a very low mobility (such as a trapped countercharge), or be another mobile charge carrier. (2) Regardless of the origin of the carriers, the electrostatic attraction between the opposite charges must be taken into account because $\gamma > 1$. This leads immediately to the conclusion that *most equilibrium charge carriers are not free in XSCs, but rather will be bound in the Coulomb well of oppositely charged ions*. Therefore, $n_d + n_a \gg n_f$. The total charge density in many XSCs may be far higher than expected based on measurements or estimates of n_f because n_a is often neglected. (3) There appears to be *no qualitative difference* between the electrostatic interactions of charges in adventitiously doped XSCs and in purposely doped XSCs. Thus, many not-purposely doped XSCs will act like purposely doped XSCs. (4) Measurements that require negligible values of n_f in an XSC, such as measuring space charge limited currents (SCLC), are unlikely to be valid in most π-conjugated polymers because of the large defect-induced charge density in this class of materials. Poole-Frenkel currents (next section) are easily mistaken for SCLC; however, PF currents are theoretically expected in doped XSC films, while SCLC are not.[64] Since SCLC theory assumes that the carrier density is at its maximum (governed by the device capacitance), it provides a lower limit to the true mobility.

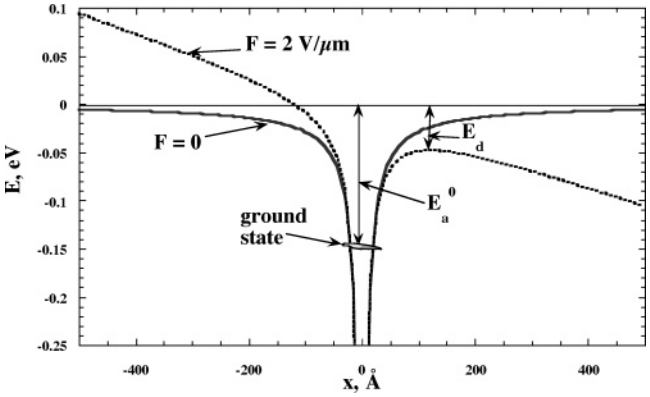

Figure 13. The activation energy for thermal emission of a charge carrier out of a Coulomb potential well decreases with the square root of the applied field, $F^{1/2}$ (Poole-Frenkel mechanism, eq 12). Therefore, the free carrier density, n_f, should be proportional to $\exp(F^{1/2}/kT)$.

The Poole-Frenkel Mechanism

The quantity of interest for transport studies is the number of free carriers, n_f, since this, and the carrier mobility, determine the observable current density. As discussed, $n_d + n_a \gg n_f$ in doped XSCs (eq 7) because $\gamma > 1$. The Poole-Frenkel (PF) mechanism proposed in 1938[17,56,58] treats the effect of an applied electric field, F, on carriers trapped in Coulomb potential wells in an isotropic solid (Figure 13). We expect this mechanism (slightly modified below) to semiquantitatively describe the $J-F$ characteristics of many purposely and adventitiously doped XSCs.

The dark current in the PF mechanism is expected to increase with $\exp(F^{1/2}/kT)$ as the field decreases the height of the electrostatic potential well surrounding the bound carrier pairs (Figure 13 and eq 12):

$$J = q\mu_n F n_d \exp((-E_a^{\,0} + (q^3/\pi\epsilon_0\epsilon)^{1/2}F^{1/2})/kT) \qquad (12)$$

Equation 12 can be derived easily by considering the factors shown in Figure 13; it is written for the simplest case (relevant to the doped LC perylene diimides) where n_d dominates J, n_a can be neglected, and where there is only a single E_a^0. The increase in current with $\exp(F^{1/2}/kT)$ occurs because n_f is proportional to $\exp(F^{1/2}/kT)$. This point is often misunderstood in the recent literature where it may be asserted that the PF

mechanism predicts an $\exp(F^{1/2}/kT)$ dependence of the *mobility*. However, Frenkel explicitly stated that "the increase in electrical conductivity in intense fields is due to the number of free electrons, and not to their mobility".[56] The failure to distinguish between the field dependences of n_f and μ_n, and to realize that *both* increase with F, is a common problem of existing models.

The PF mechanism assumes that J is controlled by the number of carriers trapped in Coulomb potential wells. Therefore, it is *not* expected to apply to molecularly doped polymers or pure crystalline XSCs in which n_f is very low.[23,36] However, in the doped perylene diimide films described earlier, where one dopant electron occurs for every cationic dopant molecule, the PF mechanism is the obvious choice for describing (at least approximately) the bulk transport-limited conductivity. And as described above, it may also apply to other XSCs in which $n_d + n_a \gg n_f$ because there appears to be no fundamental electrostatic distinction between these systems and the doped perylene diimides.

A mechanism very similar to the PF mechanism is commonly employed to describe contact-limited conductivity. The "Schottky effect" is described by an equation almost identical to eq 12: however, the second term in the exponential is just half that shown in eq 12, and E_a^0 is now interpreted as the energy barrier between the electrode Fermi level and the conduction band of the film.[58]

Field-Dependent Carrier Mobilities

The mobility of charge carriers in most XSC films increases with increasing electric field. This is independent of the often-overlooked field-assisted increase in n_f (e.g., the PF mechanism). To clearly understand transport in XSCs, we must distinguish between these two independent mechanisms which both result in a superlinear increase of J with F and which often occur together in the same material. The field-dependent mobilities are most clearly observed in disordered materials such as molecularly doped polymers in which n_f is negligible compared to n_{inj}.[35,36] In this case, the PF-like increase in n_f with field can be neglected. Models of charge transport in such disordered XSCs justify the field dependence of the carrier mobility by assuming a Gaussian distribution of hopping site energies[25,35,36] and/or by assuming a random distribution of fixed (but correlated) dipoles in the film.[23,24,53,55] These mechanisms have also been applied to the description of conducting polymers,[24,61,62,65] although the justification is not as compelling as it is for molecularly doped polymers. As suggested above (Figure 12), any disruption of the potential energy of carriers (fluctuations in conduction and valence bands) on a spatial scale larger than $2r_B$ will result in a mobility that is dependent on thermal emission of the carrier over the potential barriers or out of the potential wells. This will greatly decrease μ_n compared to the delocalized carrier case (Figure 12). The height of the potential barriers will also decrease with applied electric field. Therefore, the mobility will always be field-dependent when $2r_B <$ potential fluctuation length. The quantitative decrease in barrier height with potential depends on the *shape* of the barrier: Coulomb barriers, as assumed in the PF model, are convenient and logical in some cases, but are certainly not always correct.

Despite their highly crystalline nature, the "random dipole" mechanism may approximately apply to the mobility of carriers in the doped PPEEB films. Dipoles are formed by the electrons electrostatically bound at an average distance of r_B (eq 1) to their dopant counterions. They are free to orient in almost any direction (Figure 7) and therefore will minimize any existing *static* electric fields. In this sense, they are not the random permanent dipoles treated by the existing models. When discussing transport, however, the *rate* at which the dipoles reorient with respect to the charge hopping rate is the important parameter. Since the dipoles reorient by what is, in essence, a charge hopping process, we expect these two rates to be similar. Therefore, the dipoles will begin to reorient on the time scale of charge hopping but they will not have time to reach an equilibrium configuration. The dipole field will lag the charge hopping process. Thus, the charge carrier will experience a not-quite-random distribution of dipoles and there will be an energetic correlation between the site energies visited by the mobile charge.[23,55] This mechanism is more physically detailed than those considered previously, but it would appear to result in practically the same field-dependent mobility as described in the existing models.[6,23−25,35,36,53,55,65] Regardless of the model, it is clear that when there is a substantial dipole (or multipole) density in the XSC on a scale greater than r_B, the carrier mobility will be field-dependent. Even nominally undoped π-conjugated polymers are expected to have a large dipole density because of their high charge density (dipole density $\approx n_d + n_a$).

Empirical expressions for the field-dependent mobility have been proposed, but some are not compatible with the assumed hopping mechanism of carrier transport. A number of more sophisticated models for μ have been proposed.[17,23,55] Nevertheless, most models still treat n_f as a constant, which we argue is usually incorrect, and therefore attempt to ascribe all F- and T-dependent changes in conductivity to the mobility. It seems that a viable description of transport in XSCs in which $n_d + n_a \gg n_f$ is not yet available. Such XSCs constitute the majority of systems studied for, or already employed in, device applications. To move toward a reasonable, but only semiquantitative, description of transport in doped (purposely or not) XSCs, we employ a general equation for the mobility,[23,55]

$$\mu = \mu_0(T) \exp(\alpha(T)F^{1/2}) \qquad (13)$$

where the T-dependences of μ_0 and α are unknown and probably material-dependent. The $F^{1/2}$ dependence assumes that Coulomb wells/barriers limit the carrier mobility. The actual barrier shape, and therefore functional dependence on F, may well be material-dependent.

This equation, together with eq 12, leads to a modified form of the Poole-Frenkel equation that may account approximately for the $J-F$ characteristics of the doped LC perylene diimides described earlier, including the field dependences of both n_f and μ_n. Cases more complex than this quite ideal model system will be more difficult to describe.

$$J = qFn_d\mu_0(T)\exp(\alpha(T)F^{1/2}) \times \exp((-E_a^0 + (q^3/\pi\epsilon_0\epsilon)^{1/2}F^{1/2})/kT) \quad (14)$$

There are a number of approximations involved in eq 14. It assumes: (1) that all electrical properties are isotropic; (2) that all barriers can be described as Coulomb potentials; (3) that $n_a \approx 0$, so that J is controlled only by n_d and there is only a single relevant activation energy; and most importantly, (4) that the field-mediated coupling between n_f and μ_n can be ignored. A more correct treatment would require the numerical simulation of a coupled set of nonlinear tensor equations. We propose eq 14 only as a very approximate analytical equation describing a highly complex nonlinear problem. In the future we expect that some simplifying assumptions will be conceived and validated that will permit the simpler description of current flow in XSCs.

Conclusions

We propose a fundamental organizing principle that distinguishes conventional semiconductors (CSCs) from excitonic semiconductors (XSCs). The formation of excitons upon light absorption, rather than formation of free electron−hole pairs, is determined by the low dielectric constant and the limited spatial extent of the charge carrier wave functions in XSCs. An approximate equation that defines XSCs ($\gamma > 1$) is proposed. The same factors that result in exciton formation also determine the doping efficiency (number of free carriers per added dopant) and control the carrier mobility. Experiments on highly crystalline, precisely doped XSCs are described and related to adventitiously doped, amorphous π-conjugated polymers. The Coulomb force between charges in these low-dielectric materials is shown to be of predominant importance in the generation (via illumination or via doping) of free charge carriers. Since most carriers are electrostatically bound to a countercharge, increasing the dielectric constant of the films by addition of highly polarizable dopants leads to a superlinear increase in free carrier density. For the same reason, applying an increasing electric field results in a superlinear increase in free carrier density (Poole-Frenkel mechanism). This latter effect has often been overlooked in the description of XSCs.

The results from doping experiments in well-characterized systems can be explained entirely by spatial considerations derived from crystal structures and by electrostatic interactions between the charges. This interpretation was supported by studies of two dopants in two host matrixes. Generalization of these results to other XSCs strongly suggests that the free carrier density in many materials is only a small fraction of the total charge density, $n_d + n_a \gg n_f$. Therefore, many not-purposely doped materials, such as π-conjugated polymers, are expected to act similarly to purposely doped XSCs. That is, the free carrier density and the carrier mobility *both* will be increasing functions of both temperature and applied field. We propose an equation for the current density that approximately accounts for these dependences.

The predominant influence of Coulomb forces in XSCs affects nearly every aspect of their dark and photoelectrical properties. This has long been understood in the description of some processes, but is not yet commonly understood in the description of others. We attempt to provide a unified foundation for understanding XSCs upon which more detailed models of the individual processes can be built.

Experimental Section

PPEEB,[52] PPE_4CN,[44] and the end dopant[20] were synthesized and purified as described previously. The synthesis of the middle dopant is described here.

Synthesis of Perylene n-Type Middle Dopant Precursor. The synthesis of the middle dopant precursor is outlined in Scheme 1, and details are presented below. The synthetic strategy is similar to that which was used to prepare the previously reported end dopant precursor.[20] We have used the cyanoethylation and hydrogenation reactions to prepare several perylene diimide derivatives.[20,52] Thus, chloride **1** was prepared from diethylene glycol monomethyl ether using thionyl chloride in methylene chloride containing a catalytic amount of dimethylformamide. Cyanoethylation of dimethylaminoethanol, followed by quaternization with chloride **1**, afforded an excellent yield of ammonium salt **3**. Hydrogenation of this nitrile cleanly yielded amine **4**, which was required for preparation of the middle dopant precursor. As described for synthesis of the original dopant precursor,[20] perylene monoimide-anhydride PMPEEB reacted smoothly with the above amine to yield the desired perylene diimide middle dopant precursor.

Middle Dopant (Figure 6). The dopant precursor was reduced by one electron with sodium in THF and the resulting sodium chloride was removed as described earlier for the synthesis of the end dopant.[20]

*2-(2-Methoxyethoxy)ethyl Chloride (**1**).* Thionyl chloride (10 mL, 16.3 g, 137 mmol) was added dropwise with stirring and ice-cooling over a period of 2 h to a reaction mixture composed of diethylene glycol monomethyl ether (Aldrich 10,990-8) (10 mL, 10.1 g, 84 mmol), dimethylformamide (5 drops), and methylene chloride (100 mL). After the mixture was stirred overnight at room temperature, the resulting product mixture was concentrated under reduced pressure and distilled through a 20-cm column packed with glass beads to yield 8.4 g (72%) of colorless liquid; bp 160−162° (620 Torr). ^{1}H NMR (300 MHz, $CDCl_3$): δ 3.40 (s, 3 H, CH_3), 3.55−3.58 (m, 2 H, CH_2O), 3.63−3.69 (m, 4 H, CH_2O), 3.76 (br t, J = 7.2 Hz, 2 H, CH_2Cl).

*3-[2-(Dimethylamino)ethoxy]propanenitrile (**2**).* Sodium methoxide (50 mg) was added in one portion to a stirred reaction mixture composed of 2-(dimethylamino)-ethanol (Aldrich 39,126−3) (5.0 mL, 4.4 g, 50.mmol) and acrylonitrile (10.0 mL, 8.1 g, 152 mmol). The reaction mixture warmed spontaneously to approximately 55 ° C within 1−2 min and then slowly cooled to ambient temperature over a period of about 45 min. After the mixture was stirred for an additional 2 h at room temperature, a 0.2-mL portion of acetic acid was added to the resulting pale yellow mixture, and unreacted acrylonitrile was removed under reduced pressure. The crude product was suspended in methylene chloride and filtered through Celite to remove a yellow solid. Chromatography on silica gel (methylene chloride eluent)

Scheme 1

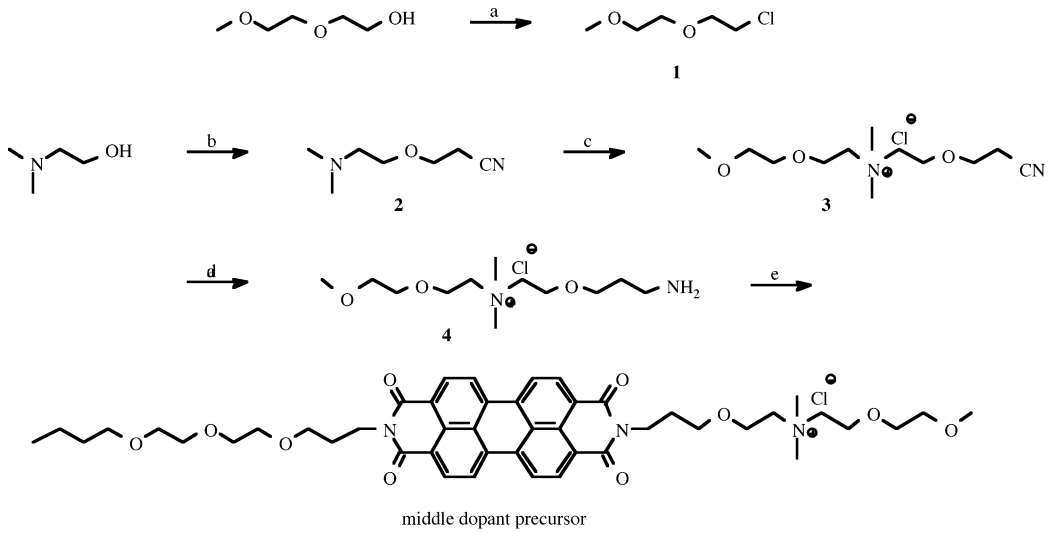

(a) $SOCl_2$ / DMF (catalytic) / CH_2Cl_2, RT
(b) CH_2=CHCN, NaOMe (catalytic), 25-55°C
(c) **1**, 65°C
(d) H_2 / PtO_2 in EtOH / $CHCl_3$, 50 psi, RT
(e) PMPEEB / pyridine, 85°C

yielded 6.4 g (90%) of pure product as a faintly yellow oil. ^{1}H NMR (300 MHz, $CDCl_3$): δ 2.28 (s, 6 H, CH_3), 2.53 (t, J = 5.7 Hz, 2 H, CH_2N), 2.63 (t, J = 6.5 Hz, 2 H, CH_2CN), 3.60 (t, J = 5.6 Hz, 2 H, NCH_2CH_2O), 3.69 (t, J = 6.6 Hz, 2 H, OCH_2CH_2CN).

*Dimethyl 2-(2-Methoxyethoxy)ethyl 2′-(2′-Cyanoethoxy)-ethylammonium Chloride (**3**).* The following reaction was performed in a 25-mL round-bottomed flask equipped with a reflux condenser, gas inlet, and magnetic stirrer bar. The reaction vessel was charged with a mixture composed of nitrile **2** (2.13 g, 15 mmol) and chloride **1** (6.95 g, 50 mmol). After the mixture was heated in an oil bath at 60−65° for 3 days, the initially homogeneous reaction mixture consisted of two separate layers. The upper layer of unreacted MEECl was removed in vacuo to yield a very viscous brownish oil. Chromatography on a silica extraction column (5−20% methanol in methylene chloride eluent) yielded 3.62 g (86%) of colorless viscous oil. ^{1}H NMR (400 MHz, $CDCl_3$): δ 2.74 (t, J = 6.0 Hz, 2 H, CH_2CN), 3.36 (s, 3 H, OCH_3), 3.46 (s, 6 H, NCH_3), 3.53−3.54 (m, 2 H, OCH_2), 3.66−3.68 (m, 2 H, OCH_2), 3.82 (t, J = 6.0 Hz, 2 H, OCH_2CH_2CN), 3.92−3.95 (m, 2 H, CH_2), 3.99−4.02 (m, 2 H, CH_2), 4.11 (br s, 2 H, CH_2).

*Dimethyl 2-(2-Methoxyethoxy)ethyl 2′-(3′-Aminopropoxy)ethylammonium Chloride (**4**).* Into a 250-mL Fisher-Porter reactor equipped with a magnetic stirring bar were placed **3** (1.17 g, 4.16 mmol), platinum oxide (100 mg), chloroform (2 mL), and absolute ethanol (100 mL). The reactor was pressurized with hydrogen gas, and the reaction mixture was stirred at room temperature for 5 days while maintaining an internal pressure of approximately 50 psi. A 1-mL portion of 15% aq NaOH (ca. 4.4 mmol) was then added, the resulting cloudy mixture was filtered through Celite, and the filtrate was concentrated on a rotary evaporator. The crude product was chromatographed on a silica extraction column (20−50% methanol in methylene chloride eluent) to yield 0.92 g (76%) of amine product as a faintly yellow viscous oil. ^{1}H NMR (400 MHz, $CDCl_3$): δ 1.72 (t, J = 6.5 Hz, 2 H, $OCH_2CH_2CH_2N$), 1.94 (br s, 2 H, NH_2), 2.76 (t, J = 6.8 Hz, 2 H, $OCH_2CH_2CH_2N$), 3.36 (s, 3 H, OCH_3), 3.48 (s, 6 H, NCH_3), 3.52−3.54 (m, 2 H, OCH_2), 3.58 (t, J = 6.2 Hz, 2 H, $OCH_2CH_2CH_2CH_3$), 3.66−3.68 (m, 2 H, OCH_2), 3.93 (br, 2 H, CH_2), 3.98−4.00 (m, 6 H, CH_2).

n-Type Middle Dopant Precursor. Into a 20-mL pressure tube (Ace Glass #8648) equipped with a magnetic stirring bar were placed **PMPEEB**[20] (50 mg, 0.08 mmol), amine **4** (55 mg, 0.17 mmol), and pyridine (2 mL). The sealed reaction mixture was heated with stirring in an oil bath at approximately 85 °C for 19 h. The resulting deep red mixture was evaporated under reduced pressure, and the crude product was purified by preparative TLC on 2-μm silica plates using 20% methanol in methylene chloride as eluent. ^{1}H NMR (300 MHz, CDCl3): δ 0.89 (t, J = 7.4 Hz, 3 H, $OCH_2CH_2CH_2CH_3$), 1.32 (br sextet, J = 7.3 Hz, 2 H, $OCH_2CH_2CH_2CH_3$), 1.54 (br quintet, J = 7.1 Hz, 2 H, $OCH_2CH_2CH_2CH_3$), 2.04−2.11 (m, 4 H, $OCH_2CH_2CH_2N$), 3.38 (*s*, 3 H, OCH_3), 3.43 (t, J = 6.8 Hz, 2 H, $OCH_2CH_2CH_2CH_3$), 3.53−3.67 (m with s at δ 3.59 and 3.63, 20 H, CH_2 and CH_3N), 3.70−3.72 (m, 2 H, OCH_2), 3.99 (br, 2 H, CH_2), 4.07−4.13 (m, 6 H, CH_2), 4.26−4.33 (m, 4 H, $OCH_2CH_2CH_2N$), 8.51 (two d, J = 8.0 Hz, 4 H, Ar−H), 8.59 (two d, J = 8.0 Hz, 4 H, Ar−H).

Acknowledgment. We are grateful to the U.S. DOE, Office of Science, Division of Basic Energy Sciences, Chemical Sciences Division for supporting this research.

References

(1) Burroughes, J. H.; Bradley, D. D. C.; Brown, A. R.; Marks, R. N.; McKay, K.; Friend, R. H.; Burns, P. L.; Holmes, A. B. *Nature* **1990**, *347*, 539.
(2) Dodabalapur, A. *Solid State Commun.* **1997**, *102*, 259.
(3) Sheats, J. R.; Antoniadis, H.; Heuschen, M.; Leonard, W.; Miller, J.; Moon, R.; Roitman, D.; Stocking, A. *Science* **1996**, *273*, 884.
(4) Zhang, X.; Jenekhe, S. A. *Macromolecules* **2000**, *33*, 2069.
(5) Garnier, F. *Chem. Phys.* **1998**, *227*, 253.
(6) Katz, H. E.; Bau, Z. *J. Phys. Chem. B* **2000**, *104*, 671.

(7) Law, K.-Y. *Chem. Rev.* **1993**, *93*, 449.
(8) Gregg, B. A.; Hanna, M. C. *J. Appl. Phys.* **2003**, *93*, 3605.
(9) Gregg, B. A. *J. Phys. Chem. B* **2003**, *107*, 4688.
(10) Wöhrle, D.; Meissner, D. *Adv. Mater.* **1991**, *3*, 129.
(11) Peumans, P.; Yakimov, A.; Forrest, S. R. *J. Appl. Phys.* **2003**, *93*, 3693.
(12) Pfeiffer, M.; Beyer, A.; Plönnigs, B.; Nollau, A.; Fritz, T.; Leo, K.; Schlettwein, D.; Hiller, S.; Wörhle, D. *Sol. Energy Mater. Sol. Cells* **2000**, *63*, 83.
(13) Jenekhe, S. A.; Yi, S. *Appl. Phys. Lett.* **2000**, *77*, 2635.
(14) Huynh, W. U.; Peng, X.; Alivisatos, A. P. *Adv. Mater.* **1999**, *11*, 923.
(15) Halls, J. J. M.; Walsh, C. A.; Greenham, N. C.; Marseglia, E. A.; Friend, R. H.; Moratti, S. C.; Holmes, A. B. *Nature* **1995**, *376*, 498.
(16) Heeger, A. J. *J. Phys. Chem. B* **2001**, *105*, 8475.
(17) Pope, M.; Swenberg, C. E. *Electronic Processes in Organic Crystals and Polymers*, 2nd ed.; Oxford University Press: New York, 1999.
(18) Smith, R. A. *Semiconductors*; Cambridge University Press: Cambridge, 1978.
(19) Fahrenbruch, A. L.; Bube, R. H. *Fundamentals of Solar Cells. Photovoltaic Solar Energy Conversion*; Academic Press: New York, 1983.
(20) Gregg, B. A.; Cormier, R. A. *J. Am. Chem. Soc.* **2001**, *123*, 7959.
(21) Jain, S. C.; Geens, W.; Mehra, A.; Kumar, V.; Aernouts, T.; Poortmans, J.; Mertens, R.; Willander, M. *J. Appl. Phys.* **2001**, *89*, 3804.
(22) Marks, T. J. *Science* **1985**, *227*, 881.
(23) Rakhmanova, S. V.; Conwell, E. M. *Appl. Phys. Lett.* **2000**, *76*, 3822.
(24) Arkhipov, V. I.; Heremans, P.; Emilianova, E. V.; Adriaenssens, G. J.; Bässler, H. *Appl. Phys. Lett.* **2003**, *82*, 3245.
(25) Bässler, H. *Phys. Status Solidi* **1993**, *175*, 15.
(26) Pfeiffer, M.; Beyer, A.; Fritz, T.; Leo, K. *Appl. Phys. Lett.* **1998**, *73*, 3202.
(27) Maennig, B.; Pfeiffer, M.; Nollau, A.; Zhou, X.; Leo, K.; Simon, P. *Phys. Rev. B* **2001**, *64*, 195208.
(28) Gregg, B. A.; Chen, S.-G.; Branz, H. M. *Appl. Phys. Lett.* **2004**, *84*, 1707.
(29) Lonergan, M. C.; Cheng, C. H.; Langsdorf, B. L.; Zhou, X. *J. Am. Chem. Soc.* **2002**, *124*, 690.
(30) Wang, Z. H.; Scherr, E. M.; MacDiarmid, A. G.; Epstein, A. J. *Phys. Rev. B* **1992**, *45*, 4190.
(31) Kaiser, A. B. *Adv. Mater.* **2001**, *13*, 927.
(32) Leempoel, P.; Fan, F.-R. F.; Bard, A. J. *J. Phys. Chem.* **1983**, *87*, 2948.
(33) Kearns, D. R.; Tollin, G.; Calvin, M. *J. Chem. Phys.* **1960**, *32*, 1020.
(34) Werner, A. G.; Li, F.; Harada, K.; Pfeiffer, M.; Fritz, T.; Leo, K. *Appl. Phys. Lett.* **2003**, *82*, 4495.
(35) Borsenberger, P. M.; Fitzgerald, J. J. *J. Phys. Chem.* **1993**, *97*, 4815.
(36) Van der Auweraer, M.; De Schryver, F. C.; Borsenberger, P. M.; Bässler, H. *Adv. Mater.* **1994**, *6*, 199.
(37) Guillemoles, J. F.; Lubomirsky, I.; Riess, I.; Cahen, D. *J. Phys. Chem.* **1995**, *99*, 14486.
(38) Simon, J.; Andre, J.-J. *Molecular Semiconductors*; Springer-Verlag: Berlin, 1985.
(39) Shen, Y.; Diest, K.; Wong, M. H.; Hsieh, B. R.; Dunlap, D. H.; Malliaras, G. G. *Phys. Rev. B* **2003**, *68*, 081204.
(40) de Leeuw, D. M. *Synth. Met.* **1993**, *57*, 3597.
(41) Jarrett, C. P.; Friend, R. H.; Brown, A. R.; de Leeuw, D. M. *J. Appl. Phys.* **1995**, *77*, 6289.
(42) Reedijk, J. A.; Martens, H. C. F.; Brom, H. B.; Michels, M. A. J. *Phys. Rev. Lett.* **1999**, *83*, 3904.
(43) Zuo, F.; Angelopoulos, M.; MacDiaramid, A. G.; Epstein, A. J. *Phys. Rev. B* **1989**, *39*, 3570.
(44) Liu, S.-G.; Sui, G.; Cormier, R. A.; Leblanc, R. M.; Gregg, B. A. *J. Phys. Chem. B* **2002**, *106*, 1307.
(45) Pearson, G. L.; Bardeen, J. *Phys. Rev.* **1949**, *75*, 865.
(46) Debye, P. P.; Conwell, E. M. *Phys. Rev.* **1954**, *93*, 693.
(47) Castellan, G. W.; Seitz, F. On the energy states of impurities in silicon. In *Semiconducting Materials*; Henisch, H. K., Ed.; Buttersworth: London, 1951.
(48) Neumark, G. F. *Phys. Rev. B* **1972**, *5*, 408.
(49) Kaneda, Y.; Stawasz, M. E.; Sampson, D., L.; Parkinson, B. A. *Langmuir* **2000**, *17*, 6185.
(50) Chen, S.-G.; Branz, H. M.; Eaton, S. S.; Taylor, P. C.; Cormier, R. A.; Gregg, B. A. *J. Phys. Chem. B* **2004**, submitted.
(51) Cormier, R., A.; Gregg, B. A. *J. Phys. Chem.* **1997**, *101*, 11004.
(52) Cormier, R. A.; Gregg, B. A. *Chem. Mater.* **1998**, *10*, 1309.
(53) Gartstein, Y. N.; Conwell, E. M. *Phys. Rev. B* **1995**, *51*, 6947.
(54) Torsi, L.; Dodabalapur, A.; Rothberg, L. J.; Fung, A. W. P.; Katz, H. E. *Science* **1996**, *272*, 1462.
(55) Novikov, S. V.; Dunlap, D. H.; Kenkre, V. M.; Parris, P. E.; Vannikov, A. V. *Phys. Rev. Lett.* **1998**, *81*, 4472.
(56) Frenkel, J. *Phys. Rev.* **1938**, *54*, 647.
(57) Verlaak, S.; Arkhipov, V. I.; Heremans, P. *Appl. Phys. Lett.* **2003**, *82*, 745.
(58) Simmons, J. G. *Phys. Rev.* **1967**, *155*, 657.
(59) Blom, P. W. M.; Vissenberg, M. C. J. M. *Mater. Sci. Eng.* **2000**, *27*, 53.
(60) Helfrich, W. Space-Charge-Limited and Volume-Controlled Currents in Organic Solids. In *Physics and Chemistry of the Organic Solid State*; Fox, D., Labes, M. M., Weissberger, A., Eds.; Interscience: New York, 1967; Vol. 3, p 1.
(61) Bozano, L.; Carter, S. A.; Scott, J. C.; Malliaras, G. G.; Brock, P. J. *Appl. Phys. Lett.* **1999**, *74*, 1132.
(62) Malliaras, G. G.; Salem, J. R.; Brock, P. J.; Scott, C. *Phys. Rev. B* **1998**, *58*, R13411.
(63) Choulis, S. A.; Nelson, J.; Kim, Y.; Poplavskyy, D.; Kreouzis, T.; Durrant, J. R.; Bradley, D. D. C. *Appl. Phys. Lett.* **2003**, *83*, 3812.
(64) Gregg, B. A. Coulomb Forces in Excitonic Solar Cells. In *Organic Solar Cells: Mechanisms, Materials and Devices*; Sun, S., Sarifciftci, S., Eds.; Marcell Dekker: New York, 2004; in press.
(65) Tanase, C.; Meijer, E. J.; Blom, P. W. M.; de Leeuw, D. M. *Phys. Rev. Lett.* **2003**, *91*, 216601.

CM049625C